Photocatalysis

Deutsche Ausgabe: DOI: 10.1002/ange.201510000
Internationale Ausgabe: DOI: 10.1002/anie.201510000

Remarkable Charge Separation and Photocatalytic Efficiency Enhancement through Interconnection of TiO_2 Nanoparticles by Hydrothermal Treatment

Yusuke Ide, Nozomu Inami, Hideya Hattori, Kanji Saito, Minoru Sohmiya, Nao Tsunoji, Kenji Komaguchi, Tsuneji Sano, Yoshio Bando, Dmitri Golberg, and Yoshiyuki Sugahara**

Abstract: *Although tremendous effort has been directed to synthesizing advanced TiO_2, it remains difficult to obtain TiO_2 exhibiting a photocatalytic efficiency higher than that of P25, a benchmark photocatalyst. P25 is composed of anatase, rutile, and amorphous TiO_2 particles, and photoexcited electron transfer and subsequent charge separation at the anatase–rutile particle interfaces explain its high photocatalytic efficiency. Herein, we report on a facile and rational hydrothermal treatment of P25 to selectively convert the amorphous component into crystalline TiO_2, which is deposited between the original anatase and rutile particles to increase the particle interfaces and thus enhance charge separation. This process produces a new TiO_2 exhibiting a considerably enhanced photocatalytic efficiency. This method of synthesizing this TiO_2, inspired by a recently burgeoning zeolite design, promises to make TiO_2 applications more feasible and effective.*

Owing to its combination of semiconducting properties with low cost, non-toxicity, and long-term stability, TiO_2 stands out as one of the most promising materials for many applications designed to deal with environmental and energy issues, including photocatalytic degradation of organic pollutants, H_2 production through photocatalytic water splitting, and photovoltaics.[1–5] When TiO_2 is used as a photocatalyst, electron–hole pairs generated by its band gap excitation are transferred to surface adsorbed substrates with competition of charge recombination; the photocatalytic efficiency of TiO_2 therefore depends largely on its charge separation efficiency, surface areas, and exposed reactive facets. Tremendous effort has thus been directed to synthesizing advanced TiO_2 particles in consideration of crystallinity (density of defects acting as recombination centers), size, porosity, and morphology.[6–11] Recently, designed TiO_2 particle interfaces have been shown to enhance the charge separation through inter-particle transfer of photoexcited electrons,[12] as well as to enhance electron mobility within dye-sensitized solar cells composed of TiO_2 mesocrystals (oriented superstructures of nanocrystal building blocks).[13] Despite this progress in advanced TiO_2 synthesis, however, it remains difficult to obtain TiO_2 that exhibits a photocatalytic efficiency higher than that of a commercial TiO_2 (P25), one of the best TiO_2 photocatalysts,[14] which has often been used as a benchmark photocatalyst.

P25 is composed of nanometer-sized particles of anatase and rutile (the main crystallographic forms of TiO_2) and amorphous TiO_2, and the anatase and rutile particles are partially interconnected.[15,16] It was pointed out that a transfer of photoexcited electrons at the rutile and anatase particle interfaces enhanced charge separation and, hence, produced a high photocatalytic efficiency.[17] Coupling of anatase and rutile particles has consequently been widely investigated as a means of enhancing the photocatalytic efficiency,[18,19] but it has remained difficult to synthesize coupled TiO_2 photocatalysts that are superior to P25. Herein, we report on a facile hydrothermal treatment of P25 to selectively dissolve the amorphous TiO_2 component and deposit crystalline TiO_2 between the partially interconnecting anatase and rutile particles, increasing the particle interfaces and thus enhancing charge separation. This treatment produces a new TiO_2 material with considerably enhanced photocatalytic efficiency. Our synthetic method was inspired by a recent

[*] Prof. Y. Ide, Prof. Y. Bando, Prof. D. Golberg
International Center for Materials Nanoarchitectonics (MANA)
National Institute for Materials Science (NIMS)
1-1 Namiki, Tsukuba, Ibaraki 305-0044 (Japan)
E-mail: IDE.Yusuke@nims.go.jp
N. Inami, K. Saito, Dr. M. Sohmiya
Department of Earth Sciences, Waseda University
1-6-1 Nishiwaseda, Shinjuku-ku, Tokyo 169–8050 (Japan)
H. Hattori, Prof. N. Tsunoji, Prof. K. Komaguchi, Prof. T. Sano
Graduate School of Engineering, Department of Applied Chemistry
Hiroshima University
1-4-1 Kagamiyama, Higashi-Hiroshima 739-8527 (Japan)
Prof. Y. Ide, Prof. Y. Sugahara
Graduate School of Creative Science and Engineering
Waseda University
1-6-1 Nishiwaseda, Shinjuku-ku, Tokyo 169–8050 (Japan)
E-mail: ys6546@waseda.jp
Prof. Y. Sugahara
Department of Applied Chemistry
School of Advanced Science and Engineering
Waseda University
3-4-1 Ohkubo, Shinjuku-ku, Tokyo 169-8555 (Japan)
and
Kagami Memorial Research Institute for Materials Science and Technology
Waseda University
2-8-26 Nishiwaseda, Shinjuku-ku, Tokyo 169-0051 (Japan)

Supporting information for this article can be found under http://dx.doi.org/10.1002/anie.201510000.

material design leveraging the chemically selective weakness of solids.[20] A good example of this approach is the synthesis of zeolites, microporous solids used as industrial catalysts, for which synthesis of specific architectures is a critical and challenging issue for attaining better performance and new applications.[21] Čejka and co-workers demonstrated that selective removal of Ge from Ge-containing zeolites composed of silica layers connected through Ge–O bonds (regioselective weakness), and then reintroduction of more Si–O bonds between the layers had produced zeolites with a range of precisely controlled pore sizes.[22] We successfully extended this material design using microscopic (inter-particle) regioselective weakness as a synthetic tool to a design using macroscopic (particle-level) regioselective weakness.

Recently,[23] we have investigated hydrothermal treatments of TiO_2-based compounds such as layered titanates using tetrapropylammonium hydroxide (TPA) and NH_4F as an alkali source to dissolve starting materials and a mineralizer to recrystallize the dissolved species, respectively.[24,25] This led to the discovery of hydrothermal conditions under which anatase and rutile are stable, whereas less chemically stable TiO_2-based compounds dissolve to recrystallize. In the present study, we treated P25 under identical conditions to selectively dissolve the amorphous TiO_2 component of P25. We named the present hydrothermal product Hyd-P25. X-ray photoelectron spectroscopy revealed that C, N, and F were not introduced into Hyd-P25 (Supporting Information, Figure S1). Small amounts of surface-adsorbed F^- were detected in Hyd-P25. This is due to residual NH_4F and thus it scarcely affects the photocatalytic activity. Scanning electron microscopy (SEM) and transmission electron microscopy (TEM) confirmed that the morphology and size of the primary particles of Hyd-P25 were almost identical to those of P25 (Figure 1 a–d and e upper). In contrast, the size of the aggregated particles of Hyd-P25 (500–600 nm), determined by dynamic light scattering (DLS) analysis (Figure 1 e lower), was considerably larger than that of P25 (200–300 nm). The specific surface area of Hyd-P25 (37 $m^2 g^{-1}$), determined by N_2 adsorption/desorption isotherms (Figure 1 f), was lower than that of P25 (50 $m^2 g^{-1}$). This supports our claim that Hyd-P25 is composed of larger aggregates than P25. This reduction in the surface area, which generally lowers the efficiency of semiconductor photocatalyst particles, did not significantly affect the photocatalytic activity of Hyd-P25 by enhancing charge separation efficiency through interconnection of the primary particles (see below).

Careful TEM observations revealed that Hyd-P25 had a larger number of particle interfaces (tight inter-particle contacts) between primary particles than P25 (yellow arrows in Figure 1 c and d). The numbers of such particle interfaces were 44 and 21 per 100 particles for Hyd-P25 and P25, respectively (Figures S2–S5). High-resolution TEM (HRTEM) revealed that Hyd-P25 contained scarcely any amorphous TiO_2 particles, which are typically observed for P25 (Figure 2 a). Composition analyses (anatase:rutile:amorphous ratio in weight) of Hyd-P25 (84:16:0) and P25 (76:13:11) using a reported method[26] supported these observations. The HRTEM image of Hyd-P25 showed the

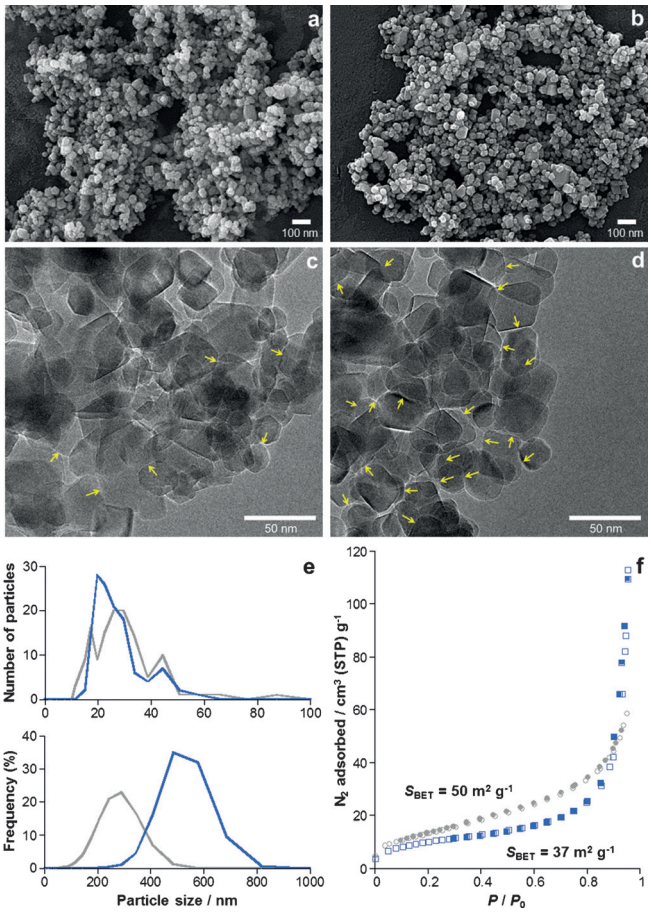

Figure 1. Morphology and structure characterizations of P25 and Hyd-P25 particles. a) SEM image of P25. b) SEM image of Hyd-P25. c) TEM image of P25. d) TEM image of Hyd-P25. e) Particle size distribution in P25 (gray lines) and Hyd-P25 (blue lines) determined by TEM (upper) and DLS (lower). f) N_2 adsorption (open)/desorption (filled) isotherms of P25 (gray) and Hyd-P25 (blue). Values in the graph are the BET surface areas of the samples.

presence of thin layers of crystalline TiO_2 between primary crystalline particles (Figure 2 b). In contrast, such layers were not observed for P25. X-ray diffraction (XRD) analysis showed that Hyd-P25 contained only anatase and rutile crystalline phases, and that the diffraction peaks relevant to anatase and rutile for Hyd-P25 were more intense than those for P25 (blue vs. gray peaks, Figure 2 c). In light of the fact that the crystallinity of anatase and rutile in P25 is probably high enough[14,27] to prevent recrystallization on their particle edges under the present relatively mild hydrothermal conditions,[23] all of the above results indicate that the amorphous TiO_2 particles in P25 were selectively dissolved to deposit anatase or rutile thin layers on the original anatase and rutile particles, and that the newly developed crystallites acted as binders to increase the particle interfaces by linking the original anatase and rutile particles. The interconnecting aggregates of anatase and rutile particles for P25[16] consequently became larger aggregated forms after the hydrothermal treatment (Figure 1 e lower). Because P25 includes up to approximately 15 wt % of amorphous TiO_2 particles,[26] we cannot rule out the possibility that the amorphous

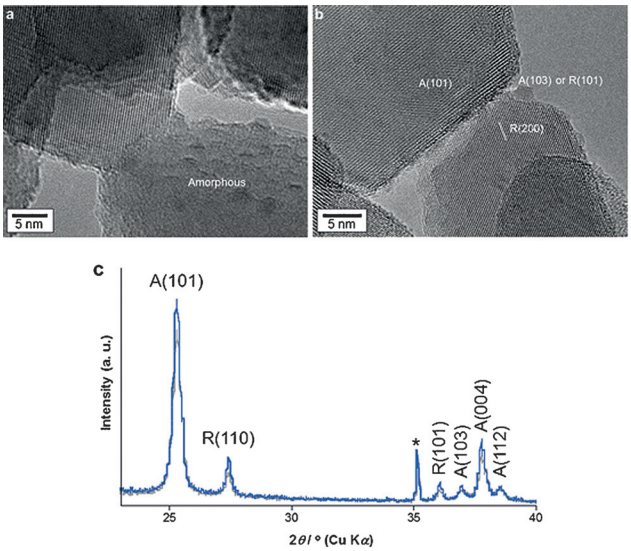

Figure 2. Characterization of amorphous TiO_2 contained in P25 and its conversion into anatase and rutile. a) HRTEM of P25. b) HRTEM of Hyd-P25. c) XRD patterns of P25 (gray line) and Hyd-P25 (blue line). The asterisk indicates a diffraction peak from Al_2O_3 used as a standard for normalizing the XRD patterns.

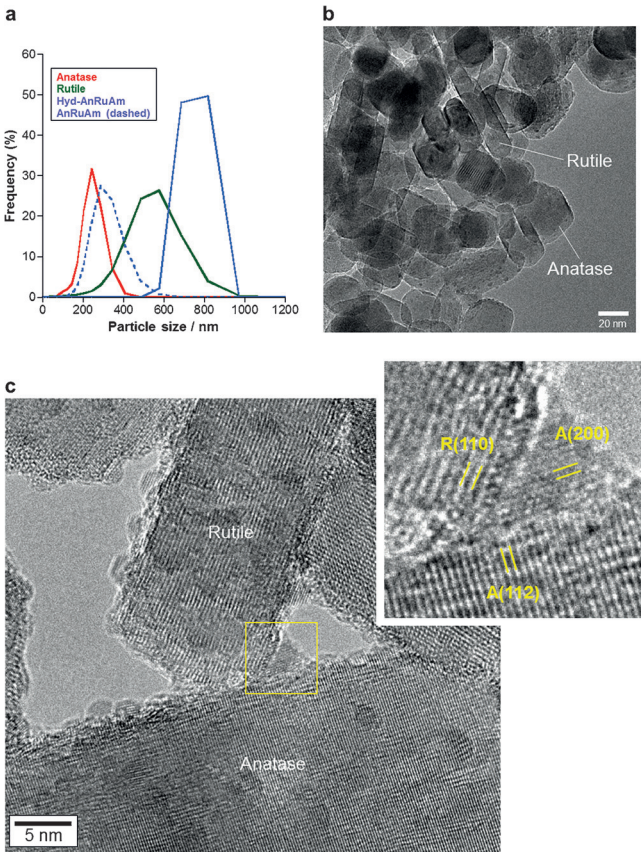

Figure 3. Control hydrothermal reactions using commercial materials of anatase, rutile, and amorphous TiO_2. a) DLS of anatase (red), rutile (green), Hyd-AnRuAm (purple), and AnRuAm (dashed purple line). b) TEM of Hyd-AnRuAm. c) HRTEM of Hyd-AnRuAm. The inset shows an expanded image of the area indicated by a yellow square.

component is converted into anatase and rutile particles whose size is almost identical to those of the primary anatase and rutile particles in P25, in addition to thin layers (Figure 2b).

Control experiments were conducted to shed light on the formation mechanism of Hyd-P25. When P25 was hydrothermally treated with either TPA or NH_4F, or without either agent, the DLS particle sizes and XRD patterns of the products were no different from those of P25. These results imply that the amorphous TiO_2 contained in P25 dissolves in a TPA alkali solution to recrystallize into anatase and rutile with the aid of NH_4F mineralizer.

To obtain a deeper understanding of the formation mechanism of Hyd-P25, additional hydrothermal experiments were conducted using commercially available anatase, rutile, and amorphous TiO_2 particles under conditions identical to those used for the synthesis of Hyd-P25. First, we hydrothermally treated only amorphous TiO_2. XRD (data not shown) and TEM (Figures S6 and S7) revealed that almost all of the amorphous phase was converted into anatase and rutile under the hydrothermal conditions (these particles were different in morphology and size from thin layers of crystalline TiO_2 observed in Hyd-P25; Figure 2b). We then hydrothermally treated a physical mixture of anatase, rutile, and amorphous TiO_2, the composition of which was identical to that reported for P25 (anatase:rutile:amorphous = 73:14:13 in weight),[26] to investigate whether amorphous TiO_2 might be selectively converted into crystalline TiO_2 to bind anatase and rutile particles into larger aggregated forms. Hydrothermal treatment of the physical mixture produced a product (Hyd-AnRuAm) with a particle size larger than that of the original anatase and rutile particles (each TiO_2 is aggregated), while the size of the untreated physical mixture (AnRuAm) was similar to that of the main anatase component, as seen in the DLS analysis (Figure 3a). TEM revealed Hyd-AnRuAm to be composed of anatase and rutile particles whose morphology and size were similar to those of the original anatase and rutile primary particles (Figure S8), with no amorphous TiO_2 particle content (Figure 3b). Moreover, HRTEM indicated that Hyd-AnRuAm had tightly contacted anatase and rutile particles that were bound by smaller TiO_2 crystallites (Figure 3c). These results support the hypotheses that the amorphous TiO_2 component of P25 also dissolves, and that the recrystallized TiO_2 thin layers bind the original anatase and rutile particles.

We further investigated the charge separation efficiency of Hyd-P25. For P25, the charges generated on rutile are separated through electron transfer to anatase trapping sites, or vice versa, between interconnecting rutile and anatase particles, and this electron transfer explains the high photocatalytic efficiency of P25.[17] Here, we compared the charge separation efficiency of Hyd-P25 and P25 by monitoring the yields of radical species, such as trapped electrons, using electron spin resonance (ESR) analysis. As shown in Figure 4a and b, when irradiated by UV light ($\lambda > 330$ nm) in the presence of molecular O_2 as an electron acceptor, Hyd-P25 created considerably larger amounts of Ti^{3+}, which were formed by trapping the photoexcited electrons. Judging from

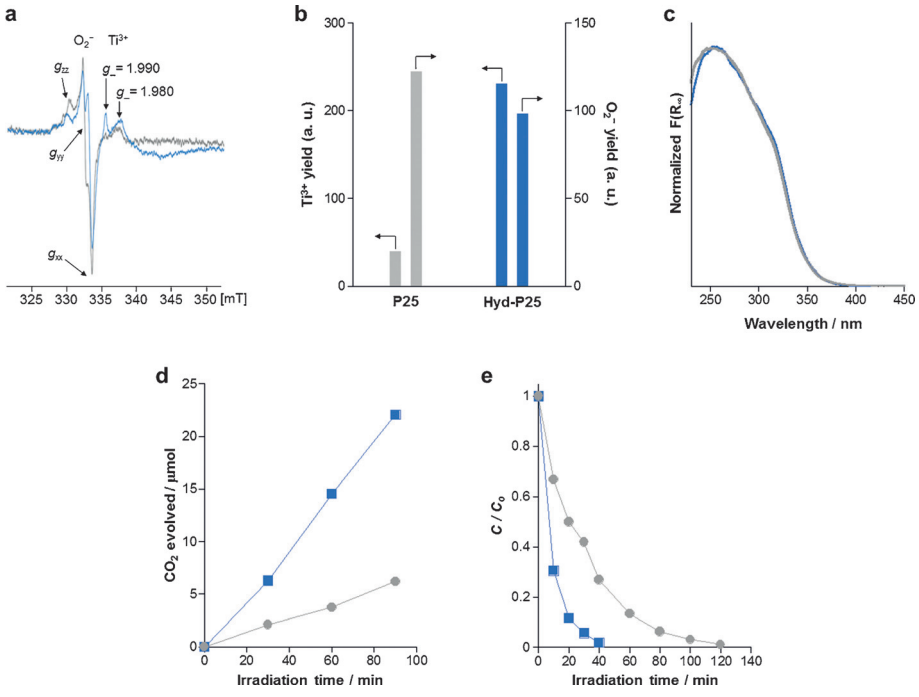

Figure 4. Photoproperties and photocatalytic performances of P25 and Hyd-P25. a) ESR spectra of P25 (gray) and Hyd-P25 (blue). b) Ti^{3+} and O_2^- yields on P25 (gray) and Hyd-P25 (blue) determined from ESR spectra. c) UV/Vis spectra of P25 (gray) and Hyd-P25 (blue). d) Time course of photocatalytic CO_2 evolution from aqueous solutions of acetic acid containing P25 (gray) and Hyd-P25 (blue) under simulated solar light irradiation ($\lambda > 300$ nm, 1 Sun). e) Time course of photodegradation of methylene blue in aqueous solutions containing P25 (gray) and Hyd-P25 (blue) under simulated solar light irradiation ($\lambda > 300$ nm, 1 Sun).

the g-values, two different Ti^{3+} types are formed in anatase for Hyd-P25. One comprises the surface electron trapping sites ($g_{\perp} = 1.980$), and the other type comprises the lattice electron trapping sites ($g_{\perp} = 1.990$).[28] Because the structural regularities of the interface TiO_2 thin layers are similar to those of the surface rather than the bulk, the notably larger amount of the former suggests that a marked increase in the number of particle interfaces plays an important role in trapping the electrons in Hyd-P25. The yields of superoxide anions (O_2^-), on the other hand, which were formed for Hyd-P25 by reduction of molecular O_2 with photoexcited electrons on the anatase surface,[29] were closely comparable to those for P25. These results indicate preferential trapping of photogenerated electrons in newly developed anatase thin layers in Hyd-P25, as well as a specific interfacial transfer of photogenerated electrons from rutile to anatase. For these reasons, photogenerated electrons and holes are separated more efficiently in Hyd-P25 than in P25. It should be noted here that the UV/Vis spectrum of Hyd-P25 was almost identical to that of P25 (Figure 4c), suggesting a close similarity in the anatase–rutile ratios, which also affects the radical species yields (amorphous TiO_2 is known to be photocatalytically inactive[30]), and thus the photocatalytic efficiency, between the two TiO_2 forms. The UV/Vis spectrum also confirmed that Hyd-P25 introduced very few elements, such as N and F, which often affect the photocatalysis of TiO_2.

As expected, Hyd-P25 showed considerably higher photocatalytic efficiency than P25. We first examined the photocatalytic activity of Hyd-P25 with respect to the oxidative decomposition of acetic acid in water to evolve CO_2, which is a well-known reaction for testing the performance of photocatalysts.[14] TiO_2 samples suspended in aerated aqueous solutions of acetic acid were irradiated by full-spectrum simulated solar light ($\lambda > 300$ nm, 1 Sun (1000 Wm^{-2}) power), allowing band gap (UV light) excitation of the TiO_2. As shown in Figure 4d, Hyd-P25 exhibited a rate of CO_2 evolution about five times higher than that of P25, which is one of the best TiO_2 photocatalysts for the reaction.[14] To our knowledge, only a small number of synthesized TiO_2 materials[6] have shown higher activity toward the reaction than P25, and the activity of Hyd-P25 is by far the highest ever reported. It should be noted here that the photocatalytic activity of Hyd-AnRuAm was nearly twice as high as AnRuAm, suggesting the versatility of the present hydrothermal reaction using chemically selective weak particles (even those added later).

We also examined the photocatalytic degradation of an organic dye, methylene blue, in water by Hyd-P25. Aqueous solutions of methylene blue containing TiO_2 photocatalysts were irradiated by 1 Sun power-simulated solar light ($\lambda >$ 300 nm). As shown in Figure 4e, photodegradation was almost complete after 40 min for Hyd-P25, whereas it took nearly 2 hours for P25 under the same testing conditions, indicating that Hyd-P25 demonstrated remarkably enhanced activity compared to P25 for this reaction as well.

It has been reported that the composition of as-supplied P25 in the same package was inhomogeneous; the amorphous phase was sometimes not found, even if the sample powder was collected from the same package.[26] In the present study, we examined the reproducibility of Hyd-P25 to find that the hydrothermal products synthesized from P25 powders collected from the same position in a package with 11 wt% of amorphous TiO_2 showed similar results with respect to syntheses, properties, and photocatalytic performance. When using P25 powders collected from another position in the same package with 6 wt% of amorphous TiO_2, on the other hand, we obtained a hydrothermal product showing a photocatalytic activity lower (ca. 70%) than Hyd-P25. These results are again indicative of the importance of amorphous TiO_2 to the interconnection of the primary particles to enhance charge separation efficiency.

In summary, we successfully synthesized a TiO_2 material, Hyd-P25, which exhibits considerably enhanced charge separation efficiency and photocatalytic efficiency by a hydro-

thermal treatment of the benchmark TiO_2 photocatalyst P25. The hydrothermal reaction involved selective dissolution of the amorphous TiO_2 component present in P25 to convert it into anatase and rutile particles that bind with the partially interconnected anatase and rutile particles to remarkably increase the particle interfaces. This approach, using chemically selective weakness (amorphous TiO_2 particles) in a powder material (P25), was inspired by a recent design of zeolites and metal–organic frameworks (MOFs), in which chemically selective weaknesses in the individual particles in a material are used to design new architectures and functions.[20] Designing TiO_2 nanoparticle interfaces, including synthesis of TiO_2 mesocrystals, has recently been a crucial issue for enhancing the charge separation efficiency and electron mobility (long-range electron connectivity) of photocatalysts and dye-sensitized solar cells, respectively.[7,12,13] Although several methodologies have been reported for such purposes, they often involve complicated procedures. The present hydrothermal method is extremely simple and offers the potential for large-scale production. Incidentally, it was reported that heating of P25 powders in air at 973 K produced anatase particles with a primary particle size and photocatalytic activity almost identical to that of P25.[31] It is thus difficult for P25 to form tight inter-particle contacts that can enhance charge separation efficiency by simple sintering at high temperatures. In addition to highly efficient photocatalysts and dye-sensitized solar cells, TiO_2 materials exhibiting long-lived charge separation can be used as visible-light-responsive photocatalysts, after surface modification, for the efficient utilization of solar or indoor light.[32] Further functionalization of Hyd-P25 and the extension of its synthetic method to other TiO_2 materials are currently under investigation in our laboratory.

Experimental Section

Hydrothermal reactions: P25 (supplied by Nippon Aerosil), TPA, H_2O, and NH_4F were mixed at a molar ratio of TiO_2:TPA:H_2O:NH_4F = 1:0.8:5:0.2 in a Teflon-lined stainless-steel autoclave, and the mixture was treated at 443 K for 7 days. The product was washed repeatedly with water and dried. Control experiments were conducted without TPA and/or NH_4F. Amorphous TiO_2 (Wako Pure Chemical) or a physical mixture of amorphous TiO_2, anatase and rutile (JRC TIO-1 and JRC TIO-6, respectively, supplied by the Catalysis Society of Japan) was also hydrothermally treated under identical conditions.

ESR analysis: ESR measurements were conducted using a JEOL JES RE-1X spectrometer (X-band). The magnetic field was calibrated and the radical yields were determined by ESR spectra recorded with a Mn^{2+}/MgO marker as an external standard reference. TiO_2 powder (10 mg) was placed in a Suprasil ESR tube (external diameter 5 mm), which was evacuated at 423 K for 1 h and cooled to room temperature. O_2 (20 torr) was introduced into the tube and retained for 10 min. The sample was photoirradiated at room temperature using a 500 W Xe lamp at $\lambda > 330$ nm for 5 min. The sample was then evacuated for 10 min to remove excess O_2 and subjected to ESR measurements at 77 K.

Photocatalytic reactions: Photocatalytic acetic acid oxidation was conducted as follows. An aqueous solution of acetic acid (5 vol%, 5 mL), saturated with molecular O_2, was mixed with TiO_2 (15 mg) in a stainless-steel container (75 mL) equipped with a Pyrex glass window by ultrasonication for 1 min, and the suspension was irradiated by a solar simulator (San-ei Electric, XES-155S1) under stirring. Acetic acid adsorption was negligible under these conditions. The headspace CO_2 was quantified by a Shimadzu GC-2010 plus gas chromatograph equipped with a BID detector. Photocatalytic degradation of methylene blue was performed as follows. A suspension containing an aqueous solution of methylene blue (0.05 ppm, 40 mL) and TiO_2 (30 mg) placed in a Pyrex glass container (50 mL) was irradiated with a solar simulator under stirring. The degree of photodegradation was measured by monitoring the changes in absorption of a methylene blue solution at 664 nm with an UV/Vis spectrometer.

Acknowledgements

This work was partly supported by JSPS KAKENHI Grant Number 26708027.

Keywords: charge separation · dye-sensitized solar cell · photocatalysis · titanium dioxide · zeolite

How to cite: *Angew. Chem. Int. Ed.* **2016**, *55*, 3600–3605
Angew. Chem. **2016**, *128*, 3664–3669

[1] A. Fujishima, X. T. Zhang, D. A. Tryk, *Surf. Sci. Rep.* **2008**, *63*, 515.
[2] A. Kudo, Y. Miseki, *Chem. Soc. Rev.* **2009**, *38*, 253.
[3] Y. Shiraishi, T. Hirai, *J. Photochem. Photobiol. C* **2008**, *9*, 157.
[4] H. Tada, T. Kiyonaga, S. Naya, *Chem. Soc. Rev.* **2009**, *38*, 1849.
[5] A. Hagfeldt, G. Boschloo, L. C. Sun, L. Kloo, H. Pettersson, *Chem. Rev.* **2010**, *110*, 6595.
[6] H. Kominami, T. Matsuura, K. Iwai, B. Ohtani, S. Nishimoto, Y. Kera, *Chem. Lett.* **1995**, 693.
[7] Z. Bian, J. Zhu, J. Wen, F. Cao, Y. Huo, X. Qian, Y. Cao, M. Shen, H. Li, Y. Lu, *Angew. Chem. Int. Ed.* **2011**, *50*, 1105; *Angew. Chem.* **2011**, *123*, 1137.
[8] H. G. Yang, C. H. Sun, S. Z. Qiao, J. Zou, G. Liu, S. C. Smith, H. M. Cheng, G. Q. Lu, *Nature* **2008**, *453*, 638.
[9] F. Amano, O. O. Prieto-Mahaney, Y. Terada, T. Yasumoto, T. Shibayama, B. Ohtani, *Chem. Mater.* **2009**, *21*, 2601.
[10] E. Bae, N. Murakami, T. Ohno, *J. Mol. Catal. A* **2009**, *300*, 72.
[11] J. M. Macak, M. Zlamal, J. Krysa, P. Schmuki, *Small* **2007**, *3*, 300.
[12] Z. Bian, T. Tachikawa, T. Majima, *J. Phys. Chem. Lett.* **2012**, *3*, 1422.
[13] E. J. W. Crossland, N. Noel, V. Sivaram, T. Leijtens, J. A. Alexander-Webber, H. J. Snaith, *Nature* **2013**, *495*, 215.
[14] O. O. Prieto-Mahaney, N. Murakami, R. Abe, B. Ohtani, *Chem. Lett.* **2009**, *38*, 238.
[15] T. Ohno, K. Sarukawa, K. Tokieda, M. Matsumura, *J. Catal.* **2001**, *203*, 82.
[16] R. I. Bickley, T. Gonzalez-Carreno, J. S. Lees, L. Palmisano, R. J. D. Tilley, *J. Solid State Chem.* **1991**, *92*, 178.
[17] D. C. Hurum, A. G. Agrios, K. A. Gray, T. Rajh, M. C. Thurnauer, *J. Phys. Chem. B* **2003**, *107*, 4545.
[18] T. Kawahara, Y. Konishi, H. Tada, N. Tohge, J. Nishii, S. Ito, *Angew. Chem. Int. Ed.* **2002**, *41*, 2811; *Angew. Chem.* **2002**, *114*, 2935.
[19] T. Ohno, K. Tokieda, S. Higashida, M. Matsumura, *Appl. Catal. A* **2003**, *244*, 383.
[20] R. E. Morris, J. Čejka, *Nat. Chem.* **2015**, *7*, 381.
[21] C. S. Cundy, P. A. Cox, *Chem. Rev.* **2003**, *103*, 663.
[22] W. J. Roth, P. Nachtigall, R. E. Morris, P. S. Wheatley, V. R. Seymour, S. E. Ashbrook, P. Chlubná, L. Grajciar, M. Položij, A. Zukal, O. Shvets, J. Čejka, *Nat. Chem.* **2015**, *7*, 628.
[23] H. Hattori, Y. Ide, T. Sano, *J. Mater. Chem. A* **2014**, *2*, 16381.

[24] S. Shibata, M. Itakura, Y. Ide, M. Sadakane, T. Sano, *Microporous Mesoporous Mater.* **2011**, *138*, 32.
[25] K. Honda, M. Itakura, Y. Matsuura, A. Onda, Y. Ide, M. Sadakane, T. Sano, *J. Nanosci. Nanotechnol.* **2013**, *13*, 3020.
[26] B. Ohtani, O. O. Prieto-Mahaney, D. Li, R. Abe, *J. Photochem. Photobiol. A* **2010**, *216*, 179.
[27] Y. Shiraishi, H. Hirakawa, Y. Togawa, Y. Sugano, S. Ichikawa, T. Hirai, *ACS Catal.* **2013**, *3*, 2318.
[28] T. Rajh, A. E. Ostafin, O. I. Micic, D. M. Tiede, M. C. Thurnauer, *J. Chem. Phys.* **1996**, *100*, 4538.
[29] M. Chiesa, M. C. Paganini, S. Livraghi, E. Giamello, *Phys. Chem. Chem. Phys.* **2013**, *15*, 9435.
[30] B. Ohtani, Y. Ogawa, S. Nishimoto, *J. Phys. Chem. B* **1997**, *101*, 3746.
[31] T. Khoa Le, D. Flahaut, H. Martinez, H. K. Hung Nguyen, T. K. Xuan Huynh, *Appl. Catal. B* **2015**, *165*, 260.
[32] Z. Bian, T. Tachikawa, P. Zhang, M. Fujitsuka, T. Majima, *J. Am. Chem. Soc.* **2014**, *136*, 458.

Received: October 26, 2015
Revised: January 28, 2016
Published online: February 17, 2016

